Available online at www.sciencedirect.com
SCIENCE DIRECT®
Physica E 21 (2004) 45–60
PHYSICA E
www.elsevier.com/locate/physe

Electronic nanodevices based on self-assembled metalloproteins

Ross Rinaldi*, Roberto Cingolani

National Nanotechnology Laboratory (NNL) of INFM, Dipartimento di Ingegneria dell'Innovazione, University of Lecce, via Arnesano, Lecce 73100, Italy

Received 27 February 2003; accepted 7 July 2003

Abstract

A key challenge of the current research in nanoelectronics is the realization of biomolecular devices. The use of electron-transfer proteins, such as the blue copper protein azurin (Az), is particularly attractive because of their natural redox properties and self assembly capability. We present in this work our results about the fabrication, characterization and modeling of devices based on such redox protein. The prototypes of biomolecular devices operate in the solid state and in air . The charge transfer process in protein devices can be engineered by using proteins with different redox centers (metal atoms) and by controlling their orientation in the solid state through different immobilization methods. A biomolecular electron rectifier has been demonstrated by interconnecting two gold nanoelectrodes with an azurin monolayer immobilized on SiO_2. The device exhibits a clear rectifying behavior with discrete current steps in the positive wing of the current–voltage curve, which are ascribed to resonant tunnelling through the redox active center. On the basis of these results we have designed an azurin-based transistor. The three terminal device exhibits an ambipolar behavior as a function of the gate bias, thus opening the way to the implementation of a new generation of logic architecture, such as fully integrated biomolecular logic gate.

Keywords: Nanotechnology; Proteins; Electronic devices

1. Introduction

In the last decade there have been dramatic advances toward the realization of molecular scale devices and integrated computers at the molecular scale [1]. First pioneering experiments were performed demonstrating that individual molecules can operate as nano-rectifiers [2], and switches [3,4] one thousand times smaller than those on conventional microchips. Very recently the assembly of tiny computer logic circuits built from such molecular scale devices has been demonstrated [5].

Researchers are working to join biology and nanotechnology, fusing useful biomolecules to chemically synthesized nanoclusters in arrangements that do everything from emitting light to storing tiny bits of magnetic data. The result is a merger of the biology's ability to assemble complex structures with the nanoscientists' capacity to build useful devices. One of the biggest drivers behind nanotechnology's enthusiasm for biological systems revolves around the organism's impressive ability to manufacture complex molecules such as DNA and proteins with atomic precision.

* Corresponding author. Tel.: +39-0832-297238; fax: +39-0832-326351.
E-mail address: ross.rinaldi@unile.it (R. Rinaldi).

1386-9477/$ - see front matter © 2003 Elsevier B.V. All rights reserved.
doi:10.1016/S1386-9477(03)00384-9

One of the fundamental goals of bioelectronics is the realization of nanoscale devices in which a few or a single biomolecule can be used to transfer and process an electronic signal. The biomolecules have particular functionality that can be exploited for the implementation of electronic devices. In order to design and realize such devices, several steps are required: (i) choice and characterization of the suitable biomolecular system, (ii) immobilization of the molecule onto an electronic substrate, (iii) interconnection to contacts, (iv) device fabrication, (v) read-out, and (vi) processing of the information. The nano bio-technology community has started a big effort along these lines to realize biomolecular devices for information technology [6]. Among biomolecules, proteins have a fundamental role in biological processes. The combination of molecular biology (for engineering proteins with the desired functional and/or self-assembling properties) and nanotechnology (for device fabrication) thus becomes the tool to realize a new class of nanoelectronic elements [7]. Different nanotechnological strategies have been selected to implement the biomolecular devices, following a bottom-up or a top-down approach depending on the biomolecule and on its functionality.

Thanks to their functional characteristics, metalloproteins appear to be good candidates for biomolecular nanoelectronics. Among them, blue copper proteins [8], and in particular azurin, are candidates of choice, due to some specific structural properties and intrinsic functionality in biological environments. They can bind gold via a disulfide site present on the protein surface, and their natural electron transfer activity can be exploited for the realization of molecular switches whose conduction state can be controlled by tuning their redox state through an external voltage source (gate). In order to realize a real biomolecular device in the solid state operating in air, a comprehensive study of the redox, electronic and electrical properties of the metalloproteins linked to an inorganic substrate under non-physiological environments must be performed [9,10]. This is crucial to enable the fabrication of the biomolecular devices, their testing and their modeling.

In this paper we describe the basic chemical–physical properties of immobilized metalloproteins, the device fabrication techniques and the basic principle of operation of the protein-based electronic devices.

2. Device fabrication

2.1. Protein monolayers

In the field of biomolecular electronics the function of proteins adsorbed at solid interfaces is of fundamental importance. Since electronic devices fabrication aims at producing a device working in air, another critical treatment is the drying procedure that can influence the protein activity. Therefore, the optimization of the chemisorption process of a protein at a surface has to be carefully developed and the protein functionality has to be checked after each step.

For the implementation of protein monolayers one has to develop surface functionalization by means of silanes, which enables the adsorption process, onto various inorganic surfaces.

Azurin [8] (Az) from *Pseudomonas aeruginosa* is a small (molecular mass 14.6 kDa, Fig. 1) and soluble metalloprotein involved in the respiratory phosphorylation of its hosting bacterium. The protein folds into an eight-stranded β-barrel motif with only a α-helix present (Fig. 1).

Given to this secondary structure and also to the presence of the disulfide bond, Az can be considered as a very stable protein. Structural and electronic

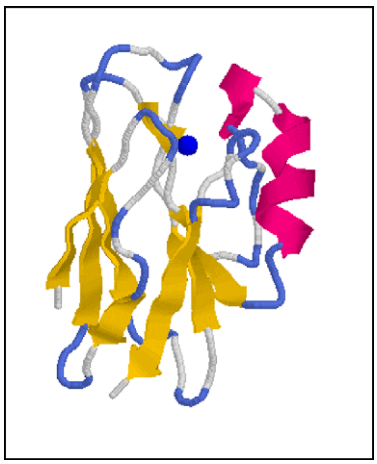

Fig. 1. Schematic structure of azurin representing eight β-barrel stands (yellow) and just one α-helix (pink).

studies have shown that the Az capability to function as a one-electron carrier, in the biological environment, is due to the equilibrium between the two stable oxidation states of the Cu ion, Cu^{1+} (reduced) and Cu^{2+} (oxidized), and to the structural stability of the active site. The redox active centre of azurin contains a copper ion liganded to five aminoacid atoms in a peculiar ligand–field symmetry, which endows the protein with unusual spectroscopic and electrochemical properties such as an intense electron absorption band at 628 nm, a small hyperfine splitting in the electron paramagnetic spectrum, and an unusually large equilibrium potential (+116 mV vs. SCE) in comparison to the Cu(II/I) aqua couple (−89 mV vs. SCE).

Commercial natural azurin from *Pseudomonas aeruginosa* (Sigma) was used without further purification after having checked that the ratio OD_{628}/OD_{280} (OD_λ = optical density measured at λ nm) was in accordance with the literature values (0.53–0.58).

Two different immobilization procedures were developed for the azurin on Si/SiO_2, exploiting different structural features of the protein and resulting in (1) random orientation (three-step procedure) and (2) oriented immobilization (two-step procedure) in the protein monolayers. Following the three-step procedure (1), the immobilization of the proteins is achieved through the formation of imido-bonds between the exposed amino groups on the azurin surface and the carbonyl heads exposed on the functionalised SiO_2 substrate. This procedure is based on a three-step chemical reaction: first, the Si/SiO_2 substrates were incubated in three-aminopropyltriethoxysilane (3-APTS) (diluted to 6.6% (V/V) in $CHCl_3$ immediately prior to use) for 2 min. and rinsed in $CHCl_3$, in order to remove 3-APTS molecules not linked to the surface; second, the sample already reacted with silanes was exposed to glutharic dialdheyde GD (diluted in H_2O to a final concentration of 4×10^{-4} M) for 10 min. and successively thoroughly washed in ultra-pure H_2O; third, the pre-coated substrates were exposed to the azurin solution for 10 min. and rinsed in NH_4Ac to get rid of physisorbed molecules. For this step a working solution of 10^{-4} M azurin in 50 mM NH_4Ac (Sigma) buffer, pH 4.6, was prepared. The buffer was degased with N_2 flow prior to use. Milli-Q grade water (resistivity 18.2 MΩcm) was used throughout all the experiments. Because the azurin molecule contains

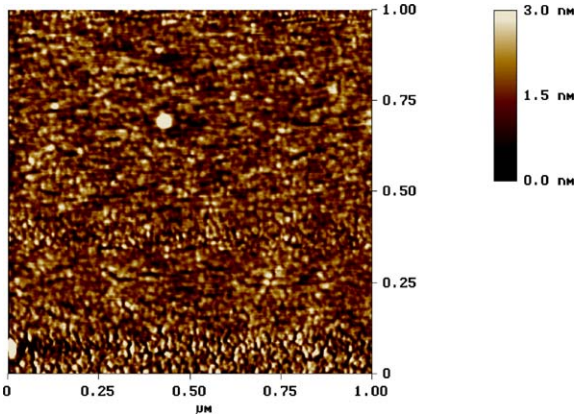

Fig. 2. Non-contact atomic force microscopy image of a self-assembled azurin monolayer, realized by means of the two step immobilization procedure.

12 surface-exposed amino groups (found in the Lys residues and in the N-terminus), random orientation of the proteins is obtained in the solid state by this immobilization method. In contrast, a highly ordered phase is achieved following procedure (2), that exploits a two-step immobilization protocol acting on the unique disulfide bond found in the protein between Cys3 and Cys26. Such a procedure not only provides a special orientation of the protein molecules, but also it facilitates the chemisorption process by avoiding the GD exposure. In this case the SiO_2 substrates were cleaved and washed with organic solvents and then incubated with H_2SO_4 and bi-distilled de-ionized water for 1 h. After washing with abundant water the substrates were incubated for 2 min. with a 2% ethanol solution of mercaptopropyltrimethoxysilane (3-MPTS) and then washed in absolute ethanol. After this step, the sample was dried under nitrogen (N_2) stream. A drop of the protein solution (0.6 μg/ml) was deposited onto the silane layer and the substrate was incubated for 5 min. at room temperature and continuously shaken in order to avoid stagnant conditions. Then it was rinsed for 5 min. with the buffer and finally with deionized water. The samples were dried under N_2 stream for non-contact atomic force microscopy (NC-AFM) imaging. A typical AFM image of azurin monolayer is displayed in Fig. 2.

Protein immobilization takes place via the reaction of the free thiol groups of 3-MPTS with the

surface disulfide bridge of Az, giving rise to substrate/overlayer disulfide bonds. By using the two-step method for the immobilization, the orientation of the molecule is expected to be well defined, as confirmed by electrochemical (cyclic voltammetry) and scanning force microscopy (SFM) measurements [11]. Samples covered just by the first molecular layers (namely 3-MPTS, 3-APTS and 3-APTS+GD) were also produced for reference.

The last procedure is specific for all those proteins with an S atom that can covalently bind the substrate. In the specific case of azurin, it exploits the presence of the disulfide bond Cys-3-Cys-26, on the protein external surface.

Synthetic wild type azurin (Az) and azurin with zinc as a metal ion and without the metal (APO form) have also been obtained using the recombinant DNA technique. The gene coding for the protein of interest has been introduced in a plasmid employed to transform *E. coli cells*. Also in this case the two step immobilization procedure was used to produce monolayers with synthetic proteins having the same orientation with respect to the substrate surface.

2.2. Morphological characterization of protein monolayers

The morphological characterization of the azurin monolayers was performed by a height distribution analysis of the AFM-images taken from azurin immobilized on SiO_2. The intrinsic loss of resolution due to the probe tip geometry has been overcome according to the method reported by Waner et al. [12], who proposed direct measurements of the heights of individual adsorbed protein molecules as the defining parameter for molecular dimensions. This approach is marginally affected by the tip geometry and it utilizes the angstrom resolution of the AFM along the vertical (z) direction [13,14]. Individual protein molecules are measured by taking the maximum height of the molecule minus the height of the local background (i.e., the uncovered substrate). Each height distribution is the average of 5–10 independent AFM images (scan size: 2 μm × 2 μm) and consists of more than 2000 individual height measurements. The fit of the experimental data is performed iteratively by means of a combination of Gaussian functions, as described by Waner et al. [12]. The centers of the Gaussian functions are taken as the measured molecular dimensions.

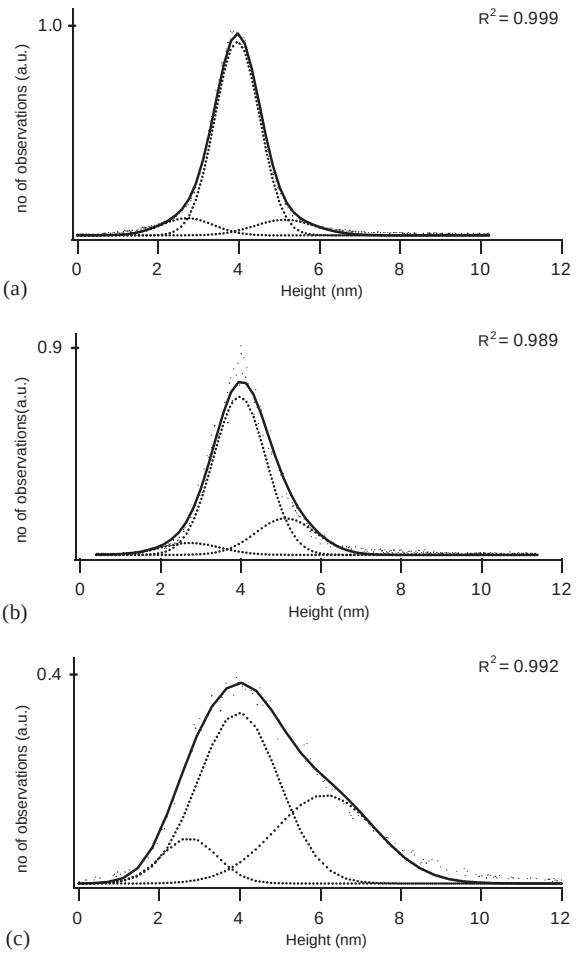

Fig. 3. AFM height distribution analysis of protein films: (a) azurin monolayer; (b) thermally treated (1 min. at 80°C) azurin monolayer; (c) thermal treatment (1 min. at 80°C) prior to immobilization.

AFM measurements on azurin monolayers (prepared from a 4×10^{-2} μM azurin solution) yielded a distribution of measured heights resulting from the convolution of three different contributions (Fig. 3a). It is noteworthy that such distribution is characterized by the presence of a main molecular species, accounting for approximately 85% of the protein population, which is centered around 4 nm, in good agreement with the reported data on azurin dimensions [15] (see also Table 1). The additional peaks in the height

Table 1
Calculated parameters of protein films according to the height distribution analysis

Species	Height (nm)	FWHM (nm)	Probability (%)
Azurin monolayer			
1	2.72 ± 0.13	1.30 ± 0.13	7.4
2	3.96 ± 0.11	1.11 ± 0.02	84.8
3	5.13 ± 0.18	1.48 ± 0.15	7.8
Thermally treated azurin monolayer			
1	2.74 ± 0.14	1.47 ± 0.15	6.3
2	3.97 ± 0.08	1.32 ± 0.12	74.2
3	5.12 ± 0.16	1.51 ± 0.18	19.5
Thermal treatment prior to immobilization			
1	2.74 ± 0.14	1.37 ± 0.16	9.9
2	3.97 ± 0.11	1.96 ± 0.14	54.8
3	6.13 ± 0.21	2.47 ± 0.22	35.3

distribution indicate the existence of two different protein species (mainly deriving from unfolded structures), possibly suggesting the formation of aggregates (5.1 nm) and proteins of smaller conformation (2.7 nm). As quoted in Table 1, these two populations account just for a small fraction of the total immobilized protein, while the intact azurin monomer seems to be the dominant contribution, demonstrating that the chemisorption process does not induce denaturation and/or conformational transitions of the azurin. This is very important, since it has been reported that the formation of aggregates may result in a significant decrease of the electron transfer rate in azurin, whereas efficient ET processes primarily require molecules retaining their proper conformation [16–18].

In order to further investigate the chemisorption process, we have performed two additional experiments in which the azurin monolayers were intentionally subjected to destructive treatments. In the first investigation, the protein films were thermally treated (hotplate, 1 min. at 80°C) before AFM measurements, and the height distribution analysis was carried out by the same technique. In the second experiment, azurin was thermally unfolded (1 min. a 80°C) before the immobilization on SiO_2, and then analyzed. The distribution of the thermally treated azurin films (Fig. 3b) shows that the prevalent species is still centered around 4 nm, but its contribution is now broader and accounts for a reduced fraction of adsorbed azurin (~74%) (Table 1). On the other hand, the other two protein populations reveal structural features which are similar to the reference film, even if the formation of aggregates seems to be increased in the heated samples. Overall, the thermal treatment of the solid state immobilized films does not seem to strongly degrade the protein conformations. This is important in view of possible high-power operation of protein transistor. A considerably different situation is found when the thermal treatment is performed in solution before the immobilization (Fig. 3c). In fact, such treatment clearly results in an adsorption mechanism with relevant conformational disorder. The monomer band (4 nm) is still present in the height distribution but, despite a significant broadening, this species contributes only for one-half of the protein structures in the film. In addition, the molecular species ascribed to larger conformations (~35% of the total population) is now centered at 6.1 nm and exhibits a strong broadening, indicating an extensive formation of multifold azurin aggregates.

All these findings demonstrate that the chemisorption process of the metalloprotein on SiO_2 via the disulphide bonds does not result in protein denaturation, since the azurin exists primarily as a monomer, hence supporting the idea that "compact" globular proteins are capable of maintaining their native structure upon adsorption.

2.3. Folding properties

The second step is to analyze the conformational properties of the immobilized azurin. In order to realize protein-based nanoscale devices in the solid state, a central problem is the proper immobilization of the molecule under non-physiological environments, so that protein folding is preserved. In particular, taking into account the strong dependence on distance of the electron transfer rate in proteins [19,20], it is fundamental that the redox centers are unperturbed upon chemisorption. Therefore, a very precise study of the conformational properties of the metalloproteins linked to the inorganic substrate is required. The conformational properties of the azurin monolayers have been investigated by intrinsic fluorescence spectroscopy. This technique provides very accurate analyses of the integrity of the protein globular

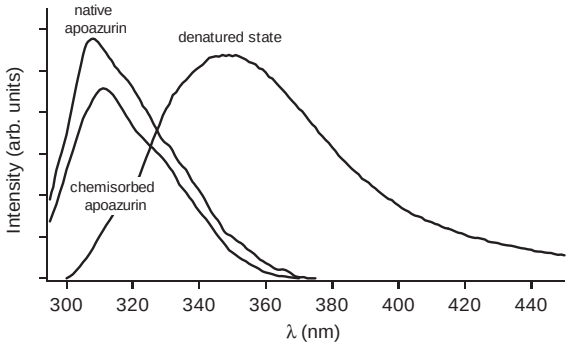

Fig. 4. Azurin fluorescence spectra : free native apoazurin, denatured apoazurin by 6 M guanidine hydrochloride, and apoazurin chemisorbed in the solid state. (The fluorescence intensities are not in scale; the spectra of the chemisorbed proteins are averaged over 10 acquisitions.)

fold, as the fluorescence parameters of the aromatic residues are highly sensitive to the microenvironment of fluorophores in protein structures [21–24]. In the following, we demonstrate that the immobilized protein does not undergo denaturation phenomena.

Azurin from *P. aeruginosa* contains a single tryptophan residue (Trp48). The fluorescence properties of Trp48 are unique, as the emission peak occurs at unusually short wavelength ($\lambda_{max} \approx 308$ nm) owing to the highly hydrophobic microenvironment surrounding it [25,15]. In the native state, azurin, apoazurin (without Cu^{2+}) and a variety of metal derivatives, such as Zn^{2+}, exhibit the same emission (and excitation) spectrum, consistent with the idea that the only structural difference stands in the metal site, as also confirmed by crystal structures determinations.

Fluorescence spectroscopy experiments were performed both in solution and in film environment in order to characterize the conformational properties of azurin molecules. It is noteworthy that, owing to the significant experimental complexity, such optical characterization represents the first direct measurement of intrinsic fluorescence from an azurin monolayer.

As reported in Fig. 4, the emission spectrum of the chemisorbed apoazurin exhibits a comparable line shape with respect to the free protein in buffer. A slight redshift (~2–3 nm) is the only minor effect detectable in the immobilized apo-protein, indicating that the covalent binding to the functionalized SiO_2 surface does not interfere with the fold pattern of the native protein. This result is supported by comparing the photoluminescence spectrum of the apo-protein monolayer with the broadband, redshifted emission of a denatured sample of azurin (6 M guanidine hydrochloride), in which the unfolding process clearly results in a large solvent exposure of hydrophobic residues that were shielded in the core of the protein in its native state. According to the photophysics of aromatic amino acids, the experimental evidence reveals that tryptophan residues in native and immobilized apo-proteins are found in similar locations. The small spectral shift suggests the possibility of a very weak internal rearrangement due to the interaction of the ligand binding, without affecting the proper fold pattern. Interestingly, also the excitation spectrum of the apo-protein was unchanged upon chemisorption, thus demonstrating the absence of any relevant perturbation in the physico-chemical conditions of the chromophore microenvironment.

Azurin contains one tryptophan (Trp48) and two tyrosines (Tyr72 and Tyr108) but, as generally recognized, its photoluminescence spectrum is basically due to Trp emission, owing to a very efficient energy transfer process between the two tyrosines and Trp48. This photophysical mechanism accounts for the fact that native azurin exhibits identical fluorescence spectra (apart from quantum yield) though excited at 270 or 295 nm, as well as identical excitation spectra for any emission wavelength. Energy transfer strongly depends on the distance between donor and acceptor chromophores and is a very sensitive probe of the protein structure. Hence, while in its native state azurin is characterized by a negligible or very small tyrosine contribution to fluorescence emission, the occurrence of externally induced conformational transitions may result in a significant decrease of the efficiency of energy transfer mechanism, and in the appearance of new spectral features which can be ascribed to tyrosine residues. This is the case, for instance, of azurin emission in acid solutions, where the unfolding action of HCl clearly results in a pronounced change of the molecular conformation [26,27]. As shown in Fig. 5a, the fluorescence spectra of apoazurin (at pH 1.5) are characterized by large redshifts of the emission maximum ($\lambda_{max} \approx 343$ nm), reflecting large solvent exposure of the aromatic residues. In particular, the fluorescence displayed in Fig. 5a are very different when excited at 270 or 295 nm (where

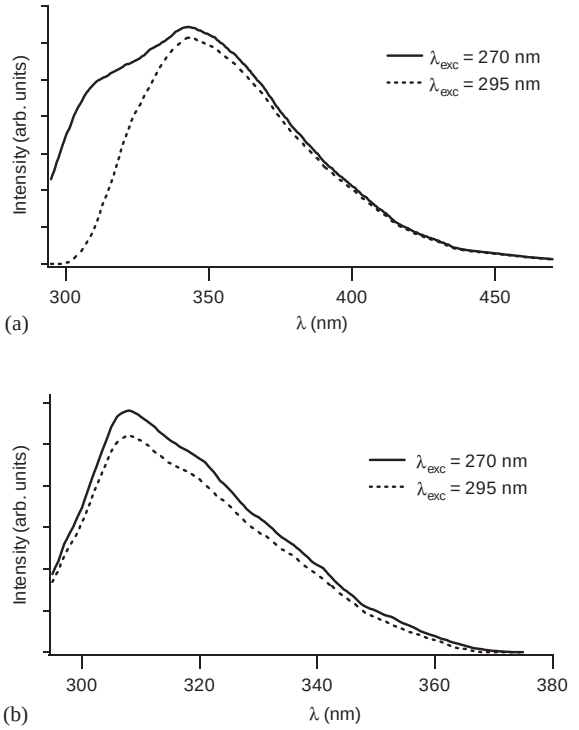

Fig. 5. (a) Free apoazurin photoluminescence at pH 1.5, excited at different wavelengths; (b) solid state apoazurin monolayers. (The fluorescence intensities are not in scale; the spectra of the chemisorbed proteins are the mean of 10 acquisitions.)

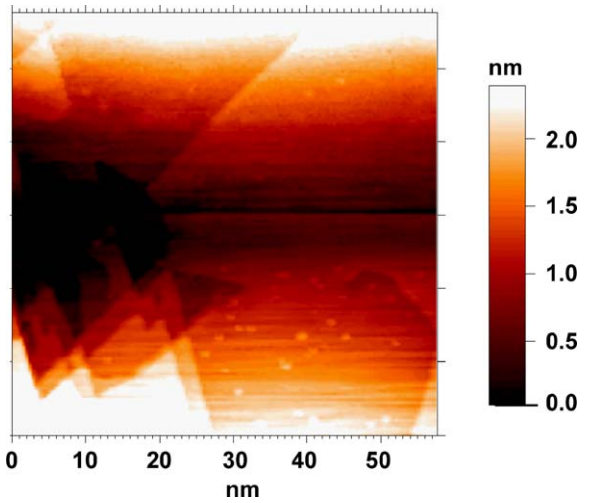

Fig. 6. STM image of an azurin monolayer onto a gold substrate (Gap voltage: −1 V; Tunneling current intensity: 0.5 nA).

tyrosine absorption is negligible), as opposed to the shape of the photoluminescence spectra for native apo-azurin (Fig. 4), which is independent on the excitation wavelength. The pronounced shoulder around 310 nm ($\lambda_{exc} \approx 270$ nm) is therefore due to tyrosine contribution, and indicates that, owing to the significant conformational changes, the transfer of excitation energy from the tyrosines to the tryptophan residue is now characterized by a very low efficiency. The same procedure was employed to further investigate the solid state azurin monolayers. In this case, however, the proper conformation retained by the chemisorbed proteins causes the photoluminescence spectra to be completely independent of the excitation wavelength, thus confirming that no variations in the folding properties occur upon immobilization. As shown in Fig. 5b, the Tyr-Trp energy transfer process was investigated by exciting the azurin films at different wavelengths and no variations in the shape of the fluorescence spectra were observed for apo-azurins (not shown). In addition, as opposed to unfolded azurin by acid pH, also the excitation spectra for light emitted at different wavelengths (300, 310, 330 and 350 nm) were identical in the molecular films, thus reflecting the same behavior of the free native protein. All these conformational features, therefore, indicate the absence of any perturbation in the folding properties of azurins upon immobilization in the solid state.

2.4. Functional state

An additional proof that chemisorption on solid surfaces via the cysteine bridge does not affect the proper folding of azurin molecules is given by STM experiments. Indeed, this technique allows us to directly investigate the electron transfer mechanism through the tunneling current, providing crucial information on the integrity of the copper active site, and, hence, on the functional state of the protein.

STM experiments were carried out, in air, on azurin Cu(II) molecules directly immobilized in the solid state onto gold substrates, exploiting its self-assembling capability on gold via the surface disulfide bridge Cys3–Cys26. Such immobilization procedure is thus analogous to that utilized for chemisorption on SiO_2. Fig. 6 shows a typical STM

image recorded with a gap voltage of −1 V and a tunneling current intensity of 0.5 nA. The proteins are clearly detectable on the gold surface as bright spots with a globular shape of size in the range of 4–6 nm, in good agreement with the reported data [15]. This finding indicates that a favorable level alignment is elicited between the Au substrate, the molecular levels of azurin and the tip, which permits electron transfer to occur through the copper active site. As expected, we found that the STM detection of the azurin at the surface was strongly dependent on the applied bias between the tip and the gold substrate, small variations of the gap voltage resulting in a complete loss of protein imaging, due to the occurrence of unstable tunneling conditions. Intramolecular ET in azurin is characterized by two main routes, the "His46 pathway" and the "Trp48 pathway", both proceeding from Cys3 to different copper-ligating residues [28]. Due to the peculiar anisotropic covalency at the active sites of blue copper proteins, the tryptophan pathway seems to be dominant [29–31]. The experimental evidence that a suitable external bias induces intramolecular ET in the immobilized protein through its intrinsic physiological pathway is thus very important, because it reveals that the azurin functionality is not lost upon immobilization. It is worth noting that this STM study represents the first experimental demonstration, obtained in air, of the possibility of inducing tunneling currents in azurin, once more confirming the very interesting perspectives for the development of hybrid nanodevices operating in non-liquid environments.

2.5. *Implementation of the two and three terminal protein-based nanodevices*

Once the chemical and physical properties of Az immobilized onto inorganic SiO_2 substrates are well assessed, the problems connected to the device fabrication can be faced.

Nanoelectrodes were fabricated by electron beam lithography (EBL) and lift-off on a Si/SiO_2 substrates. The geometry of the device comprises two planar Au/Cr contacts separated by a gap in the range 10–100 nm. For ultra narrow tip separation we developed a two-step process consisting of standard EBL and lift-off, to fabricate 100 nm separated electrodes, followed by Au electroplating deposition to reach the sub-10 nm separation. The calibration curve of the Au electroplating process (Fig. 7) shows the reduction of inter-electrode gap as a function of the electrodeposition duration. The lateral growth rate varies from 1.66 nm/s, at the beginning when the Au vertical growth is more significant, to 2.5 nm/s when the gap is reduced below 20 nm.

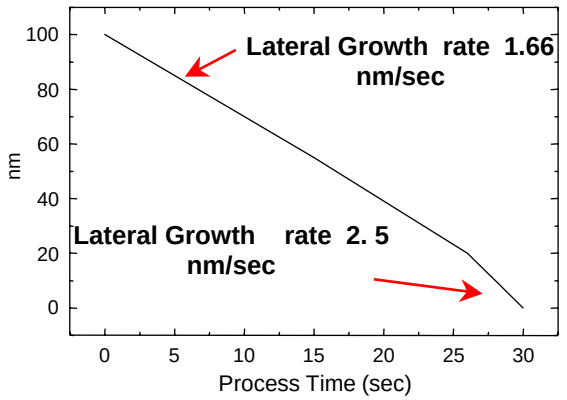

Fig. 7. Calibration curve of the Au electroplating process.

In Fig. 8 we show the high-magnification (HM) SEM images of tips obtained with EBL and lift-off followed by Au electro-deposition. By carefully adjusting the process parameters and duration, from a initial gap of 100 nm, we were able to achieve a minimum gap of only 7 ± 2 nm (Fig. 8d).

An azurin monolayer was then immobilized in the gap between the electrodes of the planar circuit by means of surface functionalization and chemisorption previously described. Both commercial natural azurin and synthetic purified azurin were used to implement the devices, following the methods described in Section 2.1. In the case of the three terminal devices the contact separation defined the gate width and a silver electrode was added on the back of the Si substrate as the gate to control the source–drain conduction. A schematic diagram of the device geometry and implementation is reported in Fig. 9. 'In the fabricated devices the incubation time of protein solution was varied in the range between 5 and 60 min. Shorter incubation times resulted in reduced surface coverage (sub-monolayer condition). In the case of two terminal devices the incubation times were in the range of 40–60 min., resulting in high current level and reduced device reproducibility and lifetime. Instead the

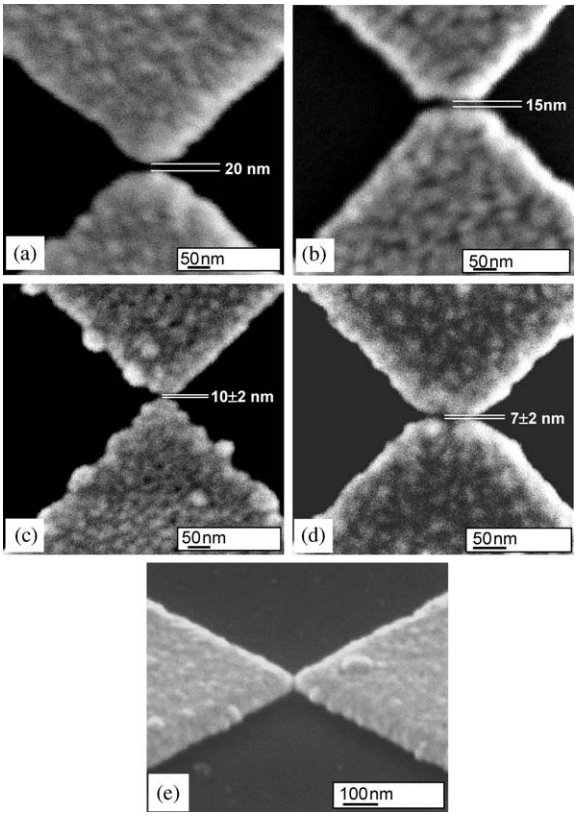

Fig. 8. HM SEM images of electrodes obtained with EBL and lift-off followed by Au electroplating deposition (process time Δt) (for all samples, the initial separation before the electrodeposition was 100 nm). (a) Cr/Au tips with separation of 20 nm (Δt=25 s); (b) Cr/Au tips with separation of 15 nm ($\Delta t = 26$ s); (c) electrodes with separation of 10 ± 2 nm ($\Delta t = 27$ s) and (d) of only 7 ± 2 nm ($\Delta t = 28$ s). (e) Cross-section SEM micrograph of electrodes with separation of 20 nm (sample tilting $\approx 60°$).

three terminal devices were produced by using incubation times no longer than 10 min. In this case the lower current level achived through a lower protein coverage decreased the sample heating and ageing during the sequence of measurements as a function of the gate voltage, thus improving the device lifetime'. All the fabricated devices were tested at room temperature and ambient pressure. Prior to protein deposition, a negative control on the empty devices was performed to check the effective insulation between the source (S) drain (D) and gate (G) terminals along the different current pathways. All these tests revealed drain–source (I_{DS}) and source–gate (I_{SG}) currents lower than 20 pA and typical open-circuit resistance larger than 100 GΩ.

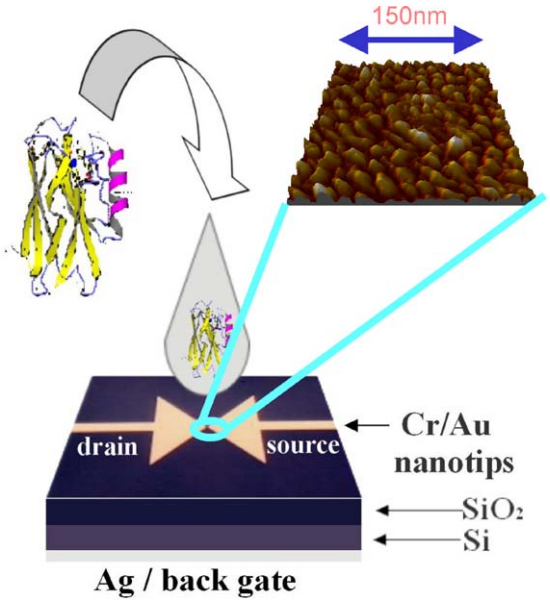

Fig. 9. A schematic diagram of the device geometry and implementation procedure. The inset shows the contact AFM image of the Az molecules immobilized onto the Si/SiO_2 substrate.

3. Nano-electronics with proteins

3.1. Two-terminal protein devices

The achievement of oriented immobilization is crucial for electronic applications in which the charge transport benefits of the long-range order of the transporting material. Orientation can in principle affect conduction in two ways: (i) it allows increased protein coverage, thus favoring electron transfer among neighboring molecules, and (ii) it enhances, for a given coverage, the intermolecular electron transfer (due to the fact that the positions of the Cu-sites are approximately coplanar, thus offering more favorable pathways for conduction).

In addition, the molecular electrostatic potential (MEP) of the protein in solution is known to be important in protein interaction properties at medium- and long distances in solution, and plays a fundamental role in the recognition processes of biomolecules. It

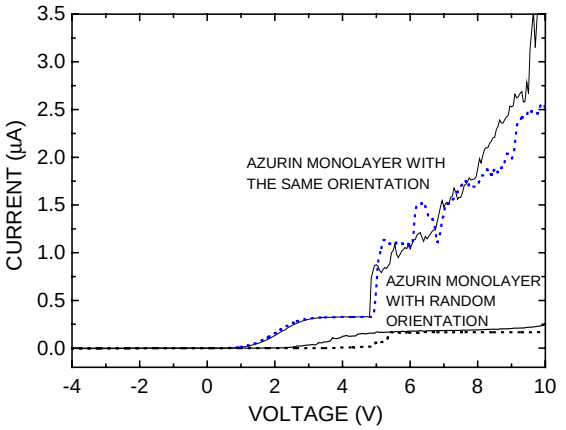

Fig. 10. Current–voltage curves of two terminal devices interconnecting proteins films with the same orientation and with random orientation. The gap between the gold electrodes was 70 nm.

is therefore expected that electrostatics will influence both the deposition kinetics of the proteins in solution, and their self-assembly. The charge distribution on the azurin surface gives origin to a strong intrinsic dipole (150 Debye), suggesting that two-terminal circuits, interconnecting solid state films of immobilized azurin molecules, should have an intrinsic polarity which depends on the value and on the orientation of the molecular dipoles. Both oriented and non-oriented azurin films should exhibit a macroscopic polarization. However, the total dipole is enhanced by depositing oriented self-assembled films with parallel dipoles. If the dipole distribution is preserved in the devices after drying, we expect that this will induce a macroscopic electric field favoring conduction.

The comparison between the current–voltage curves measured in the oriented and randomly oriented azurin layers is reported in Fig. 10. The continuous and dotted lines represent the downward and upward sweeps, respectively. Three important effects can be deduced from this comparison. Both curves are asymmetric, with a strong rectifying behavior. The value of the current measured under forward bias between the nanoelectrodes suggests that the electron transfer mechanisms in the protein, between the Cu site and the edges, is quite effective in determining the conduction processes. The difference between the positive and negative wings of the current curve of both samples may be attributed to the presence of the dipole in the azurin molecules which sets the polarization of the planar devices [9].

The current flowing through the device with the oriented layer is about 10 times larger than that flowing through the device with the non-oriented layer. As mentioned above, the regular orientation of the Az molecules, determined by the unique sticking site of the protein (the Cys3–Cys26 bridge) drives the self-assembly on the substrate, resulting in a distribution of parallel dipoles, which induces a macroscopic electric field favoring conduction. This is not the case in the sample with random orientation where parallel orientation of the molecular dipoles cannot be achieved as a consequence of the many possible sticking sites on the protein surface used in the immobilization procedure.

In the oriented protein layer under forward bias the current is step-like with a smooth exponential rise in the region between 1.9 and 2.3 V, and a steep rise around 4.9 V (Fig. 10). The step centered around 2.1 V corresponds to the energy required by the protein molecule to reduce the Cu atom by means of the electronic transition involving the S(Cys) → Cu charge-transfer. The step around 4.9 V corresponds to the energy required to perform resonant tunneling via the redox levels of azurin. Such a process occurs through a coherent two-step tunneling in which the electrons go from the negative to the positive electrode via the molecular redox level. This is consistent with the electrochemical STM measurements and in situ cyclic voltammetry curves, showing a maximum at −4.96 eV (measured with respect to the vacuum level). This step is also observable in the I–V curve of the sample with randomly oriented proteins, though less pronounced and with a small hysteresis.

In order to further elucidate the role of the metal ion and the effects of purity of the protein sample on the device performances, three different types of high-purity engineered azurins were used for implementing oriented layer devices as shown in Fig. 11 [10]:

(i) a highly purified synthetic-azurin, referred to as “recombinant azurin”, in sample (A) of Fig. 11. These proteins are identical to the natural proteins, through with a higher degree of purity;

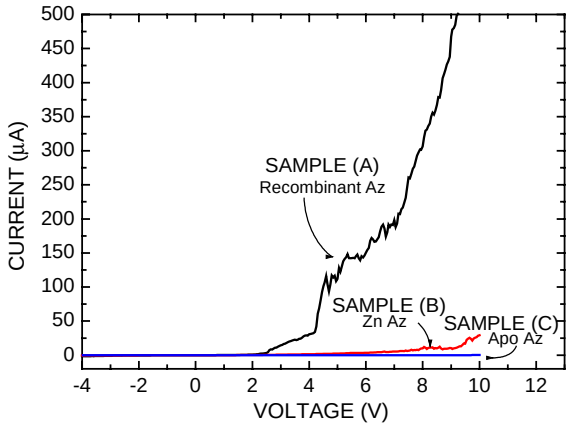

Fig. 11. Current–voltage curves of (A) recombinant Az (black), (B) Zn–Az (red), and (C) APO–Az (blue). The gap between the gold electrodes was 70 nm.

(ii) a modified synthetic azurin with the Cu atom replaced by a Zn atom (Zn–Az), in sample (B) of Fig. 11;
(iii) a modified azurin without metal atom (called APO-Az), in sample (C) of Fig. 11.

Sample (A) shows the same rectification and step-like character observed in the devices fabricated with oriented commercial (non-purified) Az layers (Fig. 10). However, the current flowing through device (A) with recombinant proteins is two orders of magnitude larger. This suggests that highly purified proteins are best suited for molecular electronic applications. Reasonably, a high degree of purification favors a closer packing of the proteins onto the device substrate and avoids passivation phenomena of the substrate. Sample (B) shows a less pronounced rectifying behavior, without the redox-induced steps characteristic of the Cu atom, and a current intensity about one order of magnitude lower than sample A. This is ascribed to the electronic properties of Zn, which are different from those of Cu. Zn has in fact only one stable redox state, Zn^{2+}, which is redox inert, thus preventing Zn–Az molecules to perform an efficient redox species-mediated electron transfer. The importance of a metal atom in the protein structure is demonstrated by device (C), which was built using APO-proteins obtained from recombinant Az. In the absence of metal redox center in the protein structure, the bio-device does not show any measurable conduction. This indicates that the metal in the protein is responsible for the electron transfer as reflected in the transport characteristics of Az biomolecular diodes.

3.2. Three-terminal protein devices

The natural electron transfer activity of the azurin can be exploited for the realization of molecular switches whose conduction state can be controlled by tuning their redox state through an external voltage source (gate).

In Fig. 12a we show the current–voltage characteristics of a protein device for drain–source voltage (V_{DS}) > 0 as a function of the gate bias (V_G) in the range between 0 and 4 V (first active region). As a general feature the drain–source current (I_{DS}) remains low (< 20 pA) up to a V_{DS} bias of about 2.3 V, and then starts to increase reaching 100 pA intensity at 6 V. A clear modulation effect is visible as a function of V_G. The dependence of I_{DS} on the V_G intensity is reported in Fig. 13a for a fixed value of V_{DS}(=4.5 V). The current increases up to a maximum value of 200 pA at $V_G = 1.1$ V, then it decreases to the 100 pA level at $V_G = 2$ V, and finally falls down to the open circuit value for higher applied gate voltages.

Similar set of measurements were performed sweeping V_{DS} from negative to positive for both positive and negative gate bias. Four different active region resulted: $V_{DS} > 0$, $V_G > 0$ (Fig. 12a); $V_{DS} > 0$, $V_G < 0$ (Fig. 12b); $V_{DS} < 0$, $V_G > 0$ (Fig. 12c); $V_{DS} < 0$, $V_G < 0$ (Fig. 12d). In Fig. 12b by decreasing the gate potential the current increases up to 160 pA at $V_{DS} = 6$ V. The corresponding dependence of the I_{DS} on V_G is reported in Fig. 13b for $V_{DS} = 5$ V. In this case we did not observe a peaked dependence, like in the case of Fig. 13a, but a smooth increase and a saturation at 115 pA in the range between -2.5 and -4 V. In the last two situations, i.e. $V_{DS} < 0$, $V_G > 0$ (Figs. 12c and 13c) and $V_{DS} < 0$, $V_G < 0$ (Figs. 12d and 13d) we observed a decrease and an increase (in absolute values) of I_{DS}, respectively, with increasing the gate voltage. As a general trend the current increases linearly for $V_{DS} \geqslant 3$ V and then saturates in the range between 4.5 and 6 V. In this voltage range the operation of the protein transistor resembles that of an inorganic MOS-FET in the saturation region,

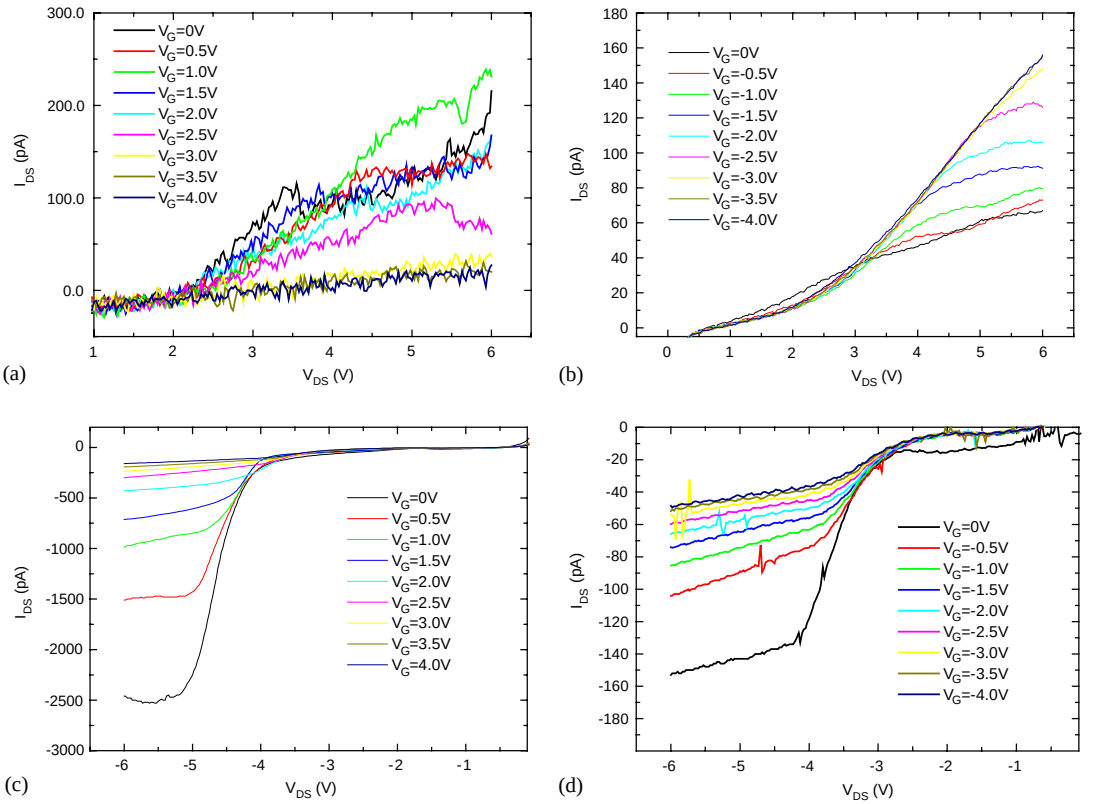

Fig. 12. I–V characteristics of the protein transistor in the four different active regions: (a) $V_{DS} > 0$, $V_G > 0$; (b) $V_{DS} > 0$, $V_G < 0$; (c) $V_{DS} < 0$, $V_G > 0$; (d) $V_{DS} < 0$, $V_G < 0$.

with constant I_{DS} for each curve. In the case of the azurin monolayer deposited in the channel of our FET, both superexchange charge transfer inside the single azurin units and sequential hopping between adjacent proteins are involved in the conduction process. The existence of a strong internal dipole due to the surface charge distribution on the protein can affect the planar conduction in the gate channel depending on whether the dipoles of the proteins in the layer are aligned or not along the source–drain axis. In the case of the characteristics of the device fabricated with commercial azurin a similar effect is observed for positive gate voltages values (Figs. 12a and c). In the case of the I–V measurements of Fig. 12c, the current intensity is higher than that of Fig. 12a, at least by a factor 10. For negative V_G the measured current intensities in the Figs. 12b and d are instead similar.

The change of the gate voltage acts in different ways depending on the versus of the bias and of the internal dipole. The I_{DS} decreases with increasing the absolute value of the applied V_G. However a different trend is usually observed in the case of $V_{DS} > 0$, $V_G > 0$ (Fig. 13a) where a peaked dependence is observed in most of the realized devices. The maximum of the current is always found around $V_G = 1$ V. This is a peculiar behavior of the protein devices which is not found in any inorganic counterpart and could be of interest for the realization of electronic devices with novel functionalities. In the case of transistors realized with synthetic and purified azurin, the current increases by a factor between 10 and 100 and the V_G resonance becomes sharper. The physical origin of this resonance can be found in the effect of the gate voltage on the molecular levels of the protein, and in turn on the conduction pathways inside the molecule.

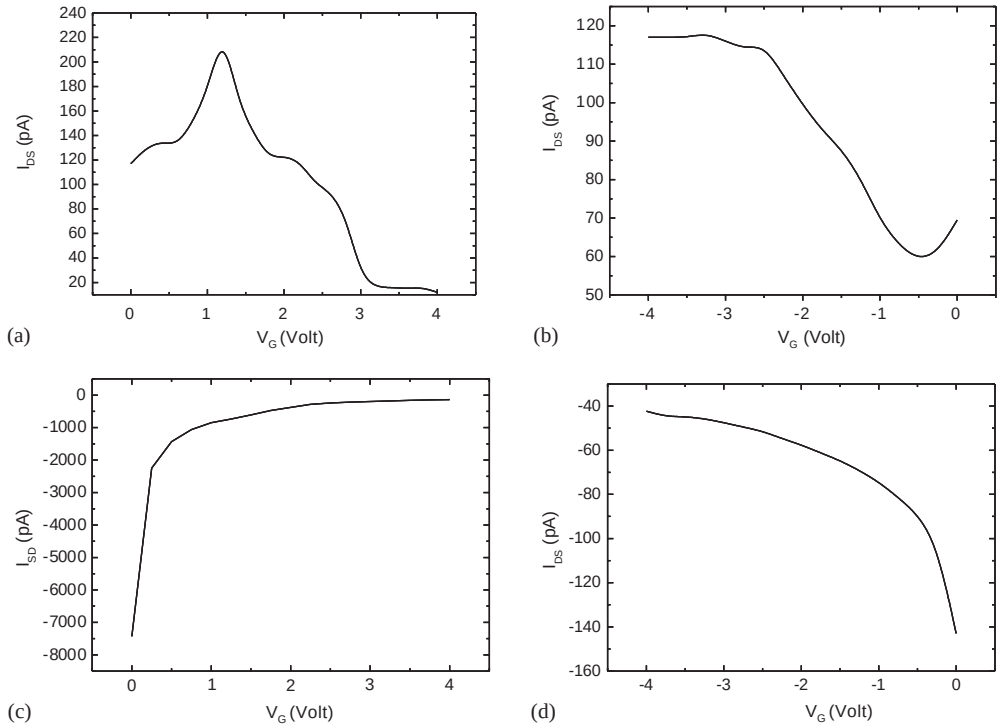

Fig. 13. I_{DS} current intensities as a function of V_G at fixed V_{DS} for the four active regions reported in Fig. 6: (a) $V_{DS} = 4.5$ V; (b) $V_{DS} = 5$ V; (c) $V_{DS} = 5$ V; (d) $V_{DS} = -5$ V.

The protein is chemisorbed onto the SiO_2 surface by the formation of a thiolate onto the silanized surface. In this way the protein sits on the surface with the axis connecting the thiolate with the Cu ion almost perpendicular to the surface. The vertical field that propagates along this direction (gate field) modifies the electronic properties of the molecule and the oxidation state of the Cu ion, since it is strongly coupled to the thiolate by the electron transfer (ET) pathway inside the protein [32]. This resonance effect has been already observed in electrochemical STM experiments [33] and in standard STM experiments performed on azurin molecules chemisorbed on Au(111) substrates at room temperature and ambient pressure.

From an electronic viewpoint, the device switches from a n-MOS FET behavior before resonance to a p-MOS FET after resonance. This is a key result because it allows us to exploit the advantages of a complementary logic, fabricating both p-type and n-type devices on the same chip. For the implementation of an inverter, the unipolar technology would require a load resistor (Fig. 14b), whereas a complementary logic (Fig. 14c)—incorporating both p-type and n-type transistor—would overcome such limitation. This results in (i) a decrease of the logic gate occupation area (reduced to the transistor-size scale); (ii) a reduction of the fabrication complexity, since in integrated circuits technology, accurate resistors are harder to make than capacitors and transistors and (iii) reduction of power consumption because, as opposed to unipolar inverters which consume power in the low state, CMOS consume power only when switching.

Our redox proteins devices are very different from standard inorganic semiconductors and conventional organic devices. Silicon MOSFETs and thin-film transistors (TFTs) are based on a gate field modulating the width and the conductance of a semiconducting channel, whereas the accepted mechanism for carbon nanotube FETs is the Schottky-barrier dominated transport. In proteins, the long-range electron transfer (ET), which represents one of the key processes of living systems involved in photosynthesis and

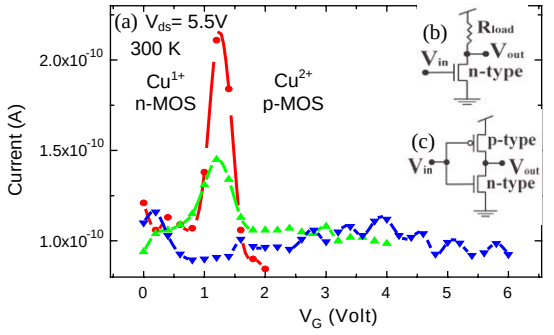

Fig. 14. (a) Transfer characteristic of the protein FET. A pronounced resonance with a Gaussian-like shape centered at $V_g = 1.25$ V is present. In this region, the transconductance changes from positive to negative values. The peak to valley ratio and the FWHM are 2 and 0.3 V, respectively. This feature gradually disappears after some cycles of measurement due to the ageing of the molecular layer (the red, green and blue curves are recorded in sequence). Insets: Electronic applications of such azurin device (b) A standard n-MOS inverter using a resistive load; (c) a CMOS inverting amplifier made with the protein FET and having the advantage of consuming power only during the switch.

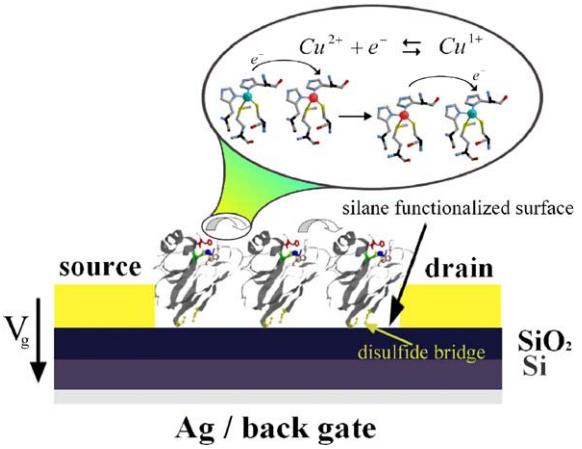

Fig. 15. Three-dimensional crystal structure of the blue-copper protein azurin containing the central Cu ion as redox site; cross section (not to scale) and transport mechanism of the protein FET. The site geometry of the copper site (the blue sphere at the top) is a distorted trigonal bipyramid one. The disulfide bridge (Cys3–Cys26, indicated in yellow at the bottom) opposite to the copper atom, is exploited to induce chemisorptions of azurins on silane-functionilazed substrates.The field effect transistor consists of a protein monolayer connecting two arrow-shaped Cr/Au electrodes on a SiO_2 substrate. An Ag back-electrode acts as the gate. As a consequence of chemiosorption, proteins sits on the surface with the electron transfer pathway—coupling the copper atom and the disulfide bridge—perpendicular to the substrate. In our model, transport is based on sequential electron hopping between one reduced azurin (blue copper ion in the inset) to an adjacent oxidized one (red ion in the inset). The gate (vertical) field influences the oxidation state of the redox site, originating the resonance.

respiration, occurs between a donor (D) and an acceptor (A) site. Two different models for ET have been proposed, i.e. a superexchange mechanism (consisting of direct quantum tunneling between the donor and the acceptor) or a sequential (incoherent) hopping between adjacent sites. The main factors influencing the ET rate are: (1) the distance between the two redox centers (electron tunneling has an exponential decrease of the ET rate with distance, whereas hopping leads to a slowly decay as the inverse of the distance); (2) the nature of the micro-environment separating the donor and acceptor (which mediates the virtual state or provides intermediate states, respectively), (3) the reorganization energy, i.e. the energy required for all structural adjustments (in the reactants and in the surrounding molecules) which are needed to assume the configuration required for the transfer of the electron and (4) the driving force. In particular, in the case of azurin, the essentially unchanged copper site geometry in the Cu^{2+} and Cu^{1+} state minimizes the reorganization energy and favors the fast electron transfer.

The transport of electrons through systems containing redox sites occurs via electron hopping from one reduced (Cu^{1+}) molecule to an adjacent oxidized (Cu^{2+}) molecule, see Fig. 15. Therefore, the presence of two adjacent Az molecules in the Cu^{1+} and Cu^{2+} redox states is required to have current flux between two planar electrodes.

In order to model the transport in the transistors, let us indicate by k_{im} the inter-molecules transfer rate. In analogy to solid state physics, we introduce two functions $f_{Cu^{1+}}$ and $f_{Cu^{2+}}$ which provide the probabilities that a copper site is in the Cu^{1+} and Cu^{2+} state, respectively (or the population of reduced and oxidized azurins in the layer). Obviously, it results $f_{Cu^{1+}} = 1 - f_{Cu^{2+}}$. Consequently, the overall electron transfer rate W_{ET} takes the form

$$\begin{aligned} W_{ET}(V_{ds}, V_g) &= k_{im}(V_{ds})G(V_g) \\ &= k_{im}(V_{ds}) f_{Cu^{2+}}(V_g) f_{Cu^{1+}}(V_g) \\ &= k_{im} f_{Cu^{2+}}(V_g)(1 - f_{Cu^{2+}}(V_g)), \end{aligned}$$

where we have assumed that V_{ds} and V_g influence k_{in} and $G = f_{Cu^{2+}}(1 - f_{Cu^{2+}})$, respectively. In other words, given the proteins and their arrangement in the layer, the inter-molecule transfer rate k_{im} only depends on the in-plane driving force, which is related to the bias applied between drain and source electrodes (hopping mechanism). On the contrary, the gate voltage only affects the electronic properties of the redox site. As a consequence of the covalent bonding on the silanized surface, the protein is chemisorbed onto the SiO_2 surface with the natural electron transfer route—which joins the copper site to the disulfide-bridge—almost perpendicular to the surface. The vertical field applied along this direction (due to V_G) modifies the oxidation state and induces a change in the equilibrium of the redox reaction, thus modifying the balance between the two populations, i.e. the probability density function $f_{Cu^{2+}}$. If we assume that at $V_g = 0$ most molecules are in the reduced state (Cu(I)), with increasing V_g the number of oxidized molecules increases, also. Therefore $df_{Cu^{2+}}/dV_g > 0$, and the relation $dG/dV_g = (dG/df_{Cu^{2+}})df_{Cu^{2+}}/dV_g = 0$ is fulfilled provided $dG/df_{Cu^{2+}} = 1 - 2f_{Cu^{2+}} = 0$, i.e. if $f_{Cu^{2+}}(V_g) = \frac{1}{2}$.

Therefore, hopping mediated electron transfer (and consequently the current as a function of V_g) is maximum when the populations of protein in the Cu^{2+} and Cu^{1+} state are equals, otherwise the current is lower. This phenomenological model explains the presence of the resonance in the transfer characteristics shown in Fig. 14. Moreover, this model is consistent with the interpretation of the redox peak in cyclic voltammetry curves and in electrochemical STM experiments performed on azurins chemiosorbed on Au(111) substrates.

4. Conclusions

We have demonstrated the first implementation of protein-based electronic nano-devices working in air and at room temperature by using azurin metalloproteins. Both rectifying (diode-like) and amplifying (transistor-like) devices have been implemented. Though this field is still in its infancy, the results obtained so far are promising and deserve further studies to determine the actual potentiality of these biodevices and to elucidate a number of important issues, such as the reproducibility and ageing of the nanodevices.

Acknowledgements

This work is a summary of recent research carried out by the *biomolecular electronics* division of the National Nanotechnology Laboratory (NNL), Lecce.

We would like to thank Giuseppe Maruccio, Adriana Biasco, Pier Paolo Pompa, Alessandro Bramanti, Valentina Arima, Paolo Visconti, Stefano D'Amico, Tonio Della Torre, Eliana D'Amone, and Diego Mangiullo. Special thanks go to the team of the European Community project SAMBA: Elisa Molinari, Rosa Di Felice, Francesca De Rienzo, Paolo Facci at S^3-INFM research center in Modena (Italy), Gerard Canters and Martin Verbeet at Leiden University (NL).

Financial support by NNL-INFM, INFM PRA project SINPROT, and by EC through SAMBA project is gratefully acknowledged.

References

[1] C. Joachim, J.K. Gimzewski, A. Aviram, Nature 408 (2000) 541.
[2] R.M. Metzger, B. Chen, U. Hopfner, M.V. Lakshmikantham, D. Vuillaume, T. Kawai, X. Wu, H. Tachibana, T.V. Hughes, H. Sakurai, J.W. Baldwin, C. Hosch, M.P. Cava, L. Brehmer, G.J. Ashwell, J. Am. Chem. Soc. 119 (1997) 10455.
[3] M.A. Reed, J. Chen, A.M. Rawlett, D.W. Price, J.M. Tour, Appl. Phys. Lett. 78 (2001) 3735.
[4] S. Roth, C. Joachim, Atomic and Molecular Wires, Kluwer, Dordrecht, 1997.
[5] K.S. Kwok, J. Ellenbogen, Mater. Today 5 (2002) 28.
[6] E. Ben-Jacob, Z. Hermon, S. Caspi, Phys. Lett. A 263 (1999) 199.
[7] I. Lee, J.W. Lee, E. Greenbaum, Phys. Rev. Lett. 79 (1997) 3294.
[8] E.T. Adman, in: P.M. Harrison (Ed.), Topics in Molecular and Structural Biology: Metalloproteins, Chemie Verlag, Weinheim, 1985.
[9] R. Rinaldi, A. Biasco, G. Maruccio, R. Cingolani, D. Alliata, L. Andolfi, P. Facci, F. De Rienzo, R. Di Felice, E. Molinari, Adv. Mater. 20 (2002) 1453.
[10] R. Rinaldi, A. Biasco, G. Maruccio, V. Arima, P. Visconti, R. Cingolani, P. Facci, F. De Rienzo, R. DiFelice, E. Molinari, M. Ph Verbeet, G.W. Canters, Appl. Phys. Lett. 82 (2003) 472.
[11] P. Facci, D. Alliata, L. Andolfi, B. Shnyder, R. Koetz, Surf. Sci. 504 (2002) 282.

[12] M.J. Waner, M. Gilchrist, M. Schindler, M. Dantus, J. Phys. Chem. B 102 (1998) 1649.
[13] A. Liu, R.C. Wu, E. Eschenazi, K. Papadopoulos, Colloids Surf. A 174 (2000) 245.
[14] M. Bergkvist, J. Carlsson, S. Oscarsson, J. Phys. Chem. B 105 (2001) 2062.
[15] H. Nar, A. Messerschmidt, R. Huber, M. van de Kamp, G.W. Canters, J. Mol. Biol. 221 (1991) 765;
H. Nar, A. Messerschmidt, R. Huber, M. van de Kamp, G.W. Canters, FEBS Lett. 306 (1992) 119;
H. Nar, R. Huber, A. Messerschmidt, A.C. Filippou, M. Barth, M. Jaquinod, M. van de Kamp, G.W. Canters, Eur. J. Biochem. 205 (1992) 1123.
[16] L. Qin, N.M. Kostic, Biochemistry 32 (1993) 6073.
[17] H.S. Pappa, S. Tajbaksh, A.J. Saunders, G.J. Pielak, T.L. Poulos, Biochemistry 35 (1996) 4837.
[18] I.M. Van Amsterdam, M. Ubbink, L.J. Jeuken, M.P. Verbeet, O. Einsle, A. Messerschmidt, G.W. Canters, Chemistry 7 (2001) 2398.
[19] C.C. Moser, P.L. Dutton, in: D.S. Bendall (Ed.), Protein Electron Transfer, Bios Scientific Publishers, Oxford, 1996, pp. 1–21.
[20] R.A. Marcus, N. Sutin, Biochim. Biophys. Acta 811 (1985) 265.
[21] M.R. Eftink, Methods Biochem. Anal. 35 (1991) 127.
[22] K. Doring, L. Konerman, L. Surrey, F. Jahnig, Eur. Biophys. J. 23 (1995) 423.
[23] J.R. Lakowicz, Principles of Fluorescence Spectroscopy, 2nd Edition, Plenum Press, New York, 1999.
[24] Y.K. Reshetnyak, E.A. Burstein, Biophys. J. 81 (2001) 1710.
[25] S.J. Kroes, G.W. Canters, G. Gilardi, A. van Hoek, A.J. Visser, Biophys J. 75 (1998) 2441.
[26] A. Finazzi-Agrò, G. Rotilio, L. Avigliano, P. Guerrieri, V. Boffi, B. Mondovi', Biochemistry 9 (1970) 2009.
[27] A. Grinvald, J. Schlessinger, I. Pecht, I.Z. Steenberg, Biochemistry 14 (1975) 1921.
[28] O. Farver, et al., Chem. Phys. 204 (1996) 271.
[29] H.E.M. Christensen, et al., Inorg. Chem. 29 (1990) 2808.
[30] M.D. Lowery, et al., J. Am. Chem. Soc. 115 (1993) 3012.
[31] S. Larsson, et al., J. Phys. Chem. 99 (1995) 4860.
[32] A.M. Kuznetsov, J. Ulstrup, Electron Transfer in Chemistry and Biology. An Introduction to the Theory, Wiley, Chichester, 1999.
[33] P. Facci, et al., Ultramicroscopy 89 (2001) 291.